Int. J. Dynam. Control (2017) 5:530–541
DOI 10.1007/s40435-016-0247-9

On coexisting bifurcations and hyperchaos in a class of diode-based oscillators: a case study

J. Kengne[1] · **M. Fouodji Tsotsop**[1,2] · **E. S. Kuetche Mbe**[2] · **H. B. Fotsin**[2] · **G. Kenne**[1]

Received: 23 November 2015 / Revised: 27 March 2016 / Accepted: 9 May 2016 / Published online: 25 May 2016

Abstract The bi-stability property and transition to hyperchaos of a class of semiconductor diode-based oscillators are investigated. A simple 4D hyperchaotic oscillator proposed by Lindberg and co-workers (referred to as the LMT oscillator hereafter) is considered as a paradigm. Due to the usage of stable oscillators coupled through a non-linear resistor, this circuit has better reproducibility and higher stability and thus may be exploited for secure communication applications. In contrast to current approaches based on piecewise-linearization methods, a smooth mathematical model is derived to investigate the dynamics of the oscillator. The bifurcation analysis shows some striking transitions including period-adding, period doubling and torus breakdown routes to chaos when monitoring the control parameters in tiny ranges. More interestingly, some regions of the parameter space corresponding to the coexistence of different attractors are revealed. This phenomenon was not reported previously and thus represents an enriching contribution concerning the behaviour of such types of oscillators. The transitions to hyperchaos are contrasted with equivalent scenarios obtained from an experimental implementation of the circuit in PSpice yielding a very good agreement.

Keywords Hyperchaotic oscillators · Shockley diode model · Bifurcation analysis · Coexistence of attractors · Basin of attraction

1 Introduction

Using hyperchaos for securing telecommunication waves is one of the most prominent applications of chaos in engineering. Hyperchaos systems are classified as chaotic systems with more than one positive Lyapunov exponent, meaning that the chaotic dynamics of the system is expanded in more than one direction leading to a more complex attractor in state space. It is well known that using hyperchaos (instead of simple chaos) for coding telecommunication signals greatly improves the degree of security (see e.g. [1] and Refs therein). Thus, the design and implementation of hyperchaos generators has remained for decades a hot topic in nonlinear science and particularly in electronics engineering. As a result, numbers of electronic circuits capable of generating hyperchaos have been proposed and investigated [2–12]. The relevant state-of-the-art provides insight/information related to the dynamic behaviour of several hyperchaotic systems [1–11]. Concerning the modelling, design and implementation of hyperchaotic electronic generators, the following most commonly used approaches can be mentioned: (a) introducing additional memory elements (followed by some structural modifications) in some conventional structures of 3D chaotic circuits [2–6]; (b) coupling of conventional chaotic oscillators [7,8]; (c) designing a universal analog computing platform to investigate hyperchaos in several types of models (e.g. Lorenz, Chua or Rössler equation) [9–12]; (d) using an infinite dimensional oscillator (i.e. delay line based circuit) [13].

✉ J. Kengne
kengnemozart@yahoo.fr

[1] Laboratoire d'Automatique et Informatique Apliquée (LAIA), IUT-FV Bandjoun, University of Dschang, Dschang, Cameroon

[2] Laboratory of Electronics and Signal Processing, Department of Physics, University of Dschang, P.O. Box 67, Dschang, Cameroon

In this paper, we consider the dynamics of a class of hyperchaotic generators including a semiconductor diode as a nonlinear element. This class includes the Matsumoto-Chua-Kobahashi hyperchaos circuit [7], the Tamasevicius-Namajunas-Cenys hyperchaos oscillator [2] and the hyperchaos circuit with damped harmonic oscillators proposed by Lindberg et al. [6], just to name a few. The common approach followed during the analysis of such oscillators is based on the piecewise-linear (PWL) description of the diode responsible for the chaos/hyperchaos behaviour of the complete electronic circuit. For instance, in the pioneering work in [6], the authors proposed a PWL model for the LMT oscillator. Based on the proposed model, the hyperchaos behaviour of the circuit was demonstrated by a numerical computation of Lyapunov exponents' spectrum. However, we stress that the PWL model represents only a first order approximation of the reality; therefore it may give rise to different types of bifurcations compared to those exhibited by the real oscillator. Furthermore, to the best of the authors' knowledge, no design tool is reported that may be exploited for a rigorous design of such types of oscillators. To overcome this drawback, this paper proposes a smooth (exponential) mathematical model [14–20] to investigate the nonlinear dynamics of this particular class of electronic oscillators using as a prototype the circuit proposed by Lindberg et al. [6] (referred to as the LMT oscillator hereafter). Various bifurcation diagrams and corresponding graphs of Lyapunov exponents are provided to define scenarios to hyperchaos and characterize the dynamics of the system in terms of the electronic circuit parameters as well. These diagrams are of precious utility for design purposes as they allow a good monitoring of the model by knowing exactly the combination of the control parameters corresponding to a regular or chaotic/hyperchaotic behaviour of the system. The idea of using the Shockley diode model (instead of its PWL approximation) followed in this paper may easily be extended to the analysis of similar types of chaos and hyperchaos generators including a diode.

The rest of the paper is structured as follows. Section 2 is concerned with the modelling process. The electronic structure of the oscillator is presented and the appropriate mathematical model is derived to describe the dynamics of the system. In Sect. 3, the fixed points of the model are determined and their stability is discussed. Section 4 focuses on the numerical analysis. Various phase portraits and bifurcation diagrams associated with their corresponding graphs of numerically computed Lyapunov exponents are plotted to explore various transitions/routes leading to chaos. Section 5 deals with the Spice simulations. The results obtained are compared with theoretical ones and a very good agreement is observed which serves to validate the model proposed in this work. Finally some concluding remarks are presented in Sect. 6.

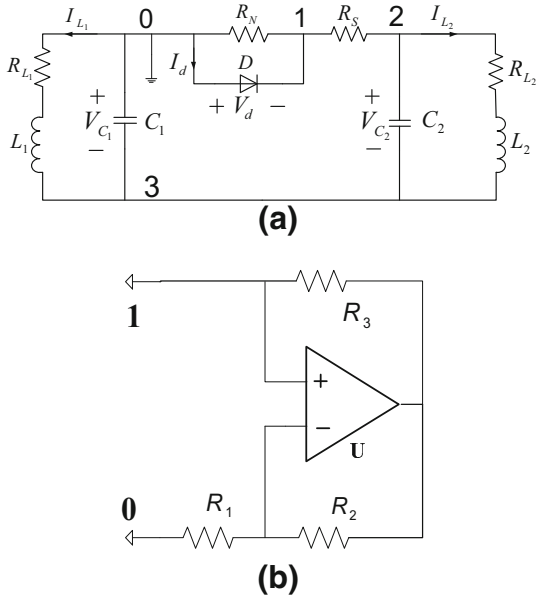

Fig. 1 Schematic diagram (**a**) of the LMT hyperchaotic oscillator [6]. The Op amplifier (**b**) with feedback resistors R_1, R_2 and R_3 (with $R_2 = R_3$) plays the role of the negative resistor (R_N) which value satisfies $R_N = -R_1$

2 Circuit description and state equations

2.1 Circuit description

The schematic diagram of the LMT oscillator [6] is depicted in Fig. 1a. The LMT oscillator includes two linear resonance circuits, (L_1, R_{L_1}, C_1) and (L_2, R_{L_2}, C_2) coupled by means of a nonlinear conductor. The nonlinear conductor is realized by a resistor R_S in series with a parallel combination of a negative impedance converter (NIC, R_N) and a general purpose semiconductor diode. The op amplifier with feedback resistors R_1, R_2, R_3 implements the negative resistor (R_N). In particular, it should be noted that for $R_2 = R_3$, the input impedance of the NIC satisfies $Z_{in} = -R_1$. In the network of Fig. 1a, b, the only nonlinear element is the diode D (assuming ideal op. amplifier implementing the NIC) whose nonlinear character is responsible for the hyperchaotic behaviour exhibited by the complete electronic circuit. It should be stressed that due to the usage of stable oscillators coupled through a nonlinear resistor, this circuit has better reproducibility and higher stability [6]. Furthermore, due to the inclusion of a large buffer resistor R_S, the circuit has lower sensitivity to the manufacturing spread of diode parameters [6].

2.2 State equations

In order to derive a mathematical model for the LMT oscillator, some useful assumptions are considered. First, we

assumed linear all capacitors, inductors and resistors (i.e. ideal op. amplifier implementing the NIC) of the oscillator network. Second, the I-V characteristic of the semiconductor diode D is modelled with an exponential function [14–18], that is:

$$I_d = f(V_d) = I_s\left[\exp(V_d/\eta V_T) - 1\right] \tag{1}$$

where V_d represents the voltage drop across the diode, I_s is the saturation current of the junction; $V_T = k_b T/q$ is the thermal voltage with k_b the Boltzmann constant; T the absolute temperature expressed in Kelvin, q the electron charge while η accounts for the ideality factor ($1 < \eta < 2$). Mention that $V_T \approx 26\,\text{mV}$ at room temperature (300 K) [12]. Denoting by I_{L_j} ($j = 1, 2$) the current flowing through the inductor L_j, and V_{C_k} ($k = 1, 2$) the voltage across capacitor C_k; the Kirchhoff's electric circuit laws can be applied to the schematic diagram of Fig. 1 to derive the following set of differential equations describing the dynamics of the LMT hyperchaotic oscillator:

$$L_1\frac{dI_{L_1}}{dt} = V_{C_1} - R_{L_1}I_{L_1} \tag{2a}$$

$$C_1\frac{dV_{C_1}}{dt} = -I_{L_1} - I_d - \frac{V_d}{R_N} \tag{2b}$$

$$L_2\frac{dI_{L_2}}{dt} = V_{C_1} - V_d - R_S I_d - \frac{R_S}{R_N}V_d - R_{L_2}I_{L_2} \tag{2c}$$

$$C_2\frac{dV_d}{dt} = \frac{-(1 + C_2/C_1)\,I_d - I_{L_1}C_2/C_1 + I_{L_2} - (1 + C_2/C_1)\,V_d/R_N}{1 + R_S/R_N + R_S dI_d/dV_d} \tag{2d}$$

where the diode current (I_d) is given by (1) and dI_d/dV_d represents its derivative with respect to V_d. It should be noted that the original state vector $\left(I_{L_1}, I_{L_2}, V_{C_1}, V_{C_2}\right)$ can still be obtained keeping in the mind that: $V_{C_2} = V_{C_1} - V_d - R_S I_d - V_d R_S/R_N$. Setting to zero the right hand side of system (2), it can be shown that the origin $\left(I_{L_1}, V_{C_1}, I_{L_2}, V_d\right)^T = (0, 0, 0, 0)^T$ is the trivial equilibrium point of the system. With the following change of variables and parameters to non dimensional form:

$$\begin{aligned} &\rho = \sqrt{L_1/C_1};\ t = \tau\sqrt{L_1C_1},\ V_{ref} = \eta V_T,\\ &x_j V_{ref} = \rho I_{L_j}\ (j = 1, 2),\ x_3 V_{ref} = V_{C_1},\ x_4 V_{ref} = V_d\\ &w = V_{C_2}/V_{ref},\ \alpha = -\frac{\rho}{R_N},\\ &\gamma_L = \frac{L_1}{L_2},\ \varepsilon_1 = \frac{R_S I_s}{V_{ref}},\ \gamma_C = \frac{C_1}{C_2},\ \varepsilon_2 = \frac{\rho I_s}{V_{ref}},\\ &\sigma_1 = \frac{R_{L_1}}{\rho},\ \sigma_2 = \frac{R_{L_2}}{\rho} \end{aligned} \tag{3}$$

the normalized circuit equations are expressed by the following smooth nonlinear fourth order differential equations:

$$\dot{x}_1 = x_3 - \sigma_1 x_1 \tag{4a}$$

$$\dot{x}_2 = \gamma_L\left(x_3 - (1 - \alpha\varepsilon_1/\varepsilon_2)\,x_4 - \sigma_2 x_2 - \varepsilon_1\varphi(x_4)\right) \tag{4b}$$

$$\dot{x}_3 = -x_1 + \alpha x_4 - \varepsilon_2\varphi(x_4) \tag{4c}$$

$$\dot{x}_4 = \frac{-x_1 + \gamma_C x_2 + \alpha\,(1 + \gamma_C)\,x_4 - (1 + \gamma_C)\,\varepsilon_2\varphi\,(x_4)}{1 - \alpha\varepsilon_1/\varepsilon_2 + \varepsilon_1\,(\varphi\,(x_4) + 1)} \tag{4d}$$

$$\varphi\,(x_4) = \exp(x_4) - 1 \tag{4e}$$

where the dots denotes differentiation with respect to τ (that we rename as t in the new scale without lost of generality). It should be noted that only one state variable (namely x_4) is involved in the exponential nonlinearity of the model in (4) and origin of the new system coordinates remains the fixed point of the model. Obviously, the model is non-symmetric (i.e. no apparent central nor axial symmetry can be captured from (4)) due to the presence of exponential nonlinearities; therefore the existence of symmetric orbits (with respect to a point or an axis) is not expected. Also note that all the state variables are real and may be captured in real experiment with a standard oscilloscope. In our model in (4), seven parameters are involved. Four of them depend on intrinsic diode parameters (i.e. ε_1 and ε_2) and the non-ideality of the inductors (i.e. σ_1 and σ_2). Consequently they will be kept constant during all the numerical computations: $\varepsilon_1 = 8.415e-6$, $\varepsilon_2 = 5.856e-5$, $\sigma_1 = 1.390e-2$, $\sigma_2 = 6.952e-3$. These parameters are obtained from (3) with the following values of electronic circuit components (inspired from Ref. 6): $L_1 = 256mH$, $C_1 = 220nF$, $R_{L1} = 15\,\Omega$, $R_{L2} = 7.5\,\Omega$, $R_S = 155\,\Omega$, $D = 1N4148(\eta = 1.9$, $V_T = 26mV$ and $I_S = 2.682nA)$. Thus, the bifurcation structures of the system will be analysed with respect to the control parameters α, γ_C and γ_L (i.e. R_N, C_2 and L_2) respectively.

We would like to stress that in contrast to the previous pioneering work [6] based on piecewise-linear (PWL) model of the LMT oscillator, the exponential model (see e.g. Ref. 20), Eq. (1), is considered throughout this paper. In fact, the PWL model is "non-smooth" and the corresponding vector field is of C^0 type while the vector field associated to the exponential model is of C^∞ type. Briefly recall that a vector field $\phi\,(x)$ is said to be of class C^k if ϕ is k-time differentiable with respect to x and the kth derivative of $\phi^{(k)}$ is continuous. Consequently, the PWL model may exhibit different types of bifurcation compared to the exponential model which it approximates [15–17].

3 Equilibrium points and their nature

It is well known that the fixed points play a crucial role on the dynamics of nonlinear systems. In this section, we deter-

mine the fixed points of the LMT hyperchaos generator and investigate their stability in terms of the model parameters.

3.1 Equilibrium points

The fixed points of system (4) can be found by solving the following nonlinear algebraic equations simultaneously:

$$x_3 - \sigma_1 x_1 = 0 \tag{5a}$$

$$\gamma_L \left(x_3 - (1 - \alpha\varepsilon_1/\varepsilon_2)\, x_4 - \sigma_2 x_2 - \varepsilon_1 \varphi(x_4)\right) = 0 \tag{5b}$$

$$-x_1 + \alpha x_4 - \varepsilon_2 \varphi(x_4) = 0 \tag{5c}$$

$$\frac{-x_1 + \gamma_C x_2 + \alpha\,(1+\gamma_C)\, x_4 - (1+\gamma_C)\,\varepsilon_2 \varphi\,(x_4)}{1 - \alpha\varepsilon_1/\varepsilon_2 + \varepsilon_1\,(\varphi\,(x_4) + 1)} = 0 \tag{5d}$$

After simple algebraic manipulations (e.g. inserting Eq. 5c in 5d), system (5) can be rewritten in the following form:

$$x_3 = \sigma_1 x_1 \tag{6a}$$

$$x_1 = \alpha x_4 - \varepsilon_2 \varphi\,(x_4) \tag{6b}$$

$$\sigma_2 x_2 = (-\sigma_1\varepsilon_2 - \varepsilon_1)\,\varphi(x_4) + (-1 + \alpha\sigma_1 + \alpha\varepsilon_1/\varepsilon_2)\, x_4 \tag{6c}$$

$$x_2 + \alpha x_4 - \varepsilon_2 \varphi\,(x_4) = 0 \tag{6d}$$

Combining Eq. (6c) and (6d), we found that the fixed points are solutions of the following transcendental equation:

$$\exp\,(x_4) - 1 = \frac{-1 + \alpha\varepsilon_1/\varepsilon_2 + \alpha\sigma_1 + \alpha\sigma_2}{\varepsilon_1 + \varepsilon_2\,(\sigma_1 + \sigma_2)} x_4 \tag{7}$$

It is clear that the number of fixed points depends on the number of solutions of Eq. (7). Obviously $P_0\,(0, 0, 0, 0)$ is a trivial solution. It can be seen that a non trivial solution may exist depending on the sign of the multiplicative term $(-1 + \alpha\varepsilon_1/\varepsilon_2 + \alpha\sigma_1 + \alpha\sigma_2)$ that appear in Eq. (7): a) If $-1 + \alpha\varepsilon_1/\varepsilon_2 + \alpha\sigma_1 + \alpha\sigma_2 \geq 0$ (i.e. $\alpha \geq \frac{1}{\sigma_1+\sigma_2+\varepsilon_1/\varepsilon_2} = \alpha_{\max}$) there exists a nontrivial solution P_1 which can be computed numerically by using for instance the MATLAB software build-in function "fzero"; b) If $-1 + \alpha\varepsilon_1/\varepsilon_2 + \alpha\sigma_1 + \alpha\sigma_2 \leq 0$ (i.e. $\alpha \leq \alpha_{\max}$) there exists a single equilibrium point $P_0\,(0, 0, 0, 0)$ for system (4). Only the latter case corresponds to realistic operation conditions of the LMT hyperchaotic oscillator and will be considered hereafter. In fact, $\alpha_{\max} = 6.0773$ with the values of system parameters mentioned in Sect. 2.2, whereas $0 \leq \alpha \leq 0.70$ for a proper operation of the oscillator (see Sect. 4). Briefly recall that an equilibrium point is simply a DC solution of the equivalent circuit and may also be determined by short-circuiting the inductors (L_1, L_2) and open-circuiting the capacitors (C_1, C_2).

3.2 Nature of the trivial fixed point

By perturbing Eq. (4) around the critical point $P_0\,(0, 0, 0, 0)$, we obtain the following 4×4 Jacobian matrix:

$$M_J = \begin{bmatrix} -\sigma_1 & 0 & 1 & 0 \\ 0 & -\sigma_2\gamma_L & \gamma_L & -\gamma_L\Gamma_0 \\ -1 & 0 & 0 & \alpha - \varepsilon_2 \\ \frac{-1}{\Gamma_0} & \frac{\gamma_C}{\Gamma_0} & 0 & \frac{\Gamma_1}{\Gamma_0} \end{bmatrix} \tag{8a}$$

$$\Gamma_0 = 1 - \alpha\varepsilon_1/\varepsilon_2 + \varepsilon_1 \tag{8b}$$

$$\Gamma_1 = (1 + \gamma_c)\,(\alpha\,(1 - \alpha\varepsilon_1/\varepsilon_2) + 2\alpha\varepsilon_1 - \varepsilon_2 - \varepsilon_1\varepsilon_2) \tag{8c}$$

Thus the stability of the trivial equilibrium point $P_0\,(0, 0, 0, 0)$ is determined according to the real parts of the roots of the following characteristic equation ($\det\,(M_J - \lambda I_d) = 0$):

$$c_4\lambda^4 + c_3\lambda^3 + c_2\lambda^2 + c_1\lambda + c_0 = 0 \tag{9a}$$

where I_d is the 4×4 identity matrix and the coefficients c_i $(i = 0, 1, 2, 3, 4)$ are defined as:

$$c_0 = \gamma_L\,(\alpha\sigma_2 - \varepsilon_2\sigma_2 - \alpha\sigma_1\gamma_c + \sigma_1\varepsilon_2\gamma_c + \gamma_c\Gamma_0 - \sigma_2\Gamma_1) \tag{9b}$$

$$c_1 = \alpha - \varepsilon_2 - \alpha\gamma_c\gamma_L + \varepsilon_2\gamma_c\gamma_L + \gamma_c\gamma_L\Gamma_0\sigma_1 - \Gamma_1 - \Gamma_1\gamma_L\sigma_1\sigma_2 + \sigma_2\gamma_L\Gamma_0 \tag{9c}$$

$$c_2 = \gamma_L\gamma_c\Gamma_0 - \sigma_2\Gamma_1\gamma_L - \sigma_1\Gamma_1 + \Gamma_0 + \sigma_2\sigma_1\gamma_L\Gamma_0 \tag{9d}$$

$$c_3 = -\Gamma_1 + \sigma_2\gamma_L\Gamma_0 + \sigma_1\Gamma_0 \tag{9e}$$

$$c_4 = \Gamma_0 \tag{9f}$$

A set of necessary and sufficient conditions for all the roots of Eq. (9) to have negative real parts is given by the well-known Routh-Hurwitz criterion expressed in the form:

$$c_i > 0\,(i = 0, 1, 2, 3, 4) \tag{10a}$$

$$c_3c_2 - c_1c_4 > 0 \tag{10b}$$

$$c_1\,(c_2c_3 - c_1c_4) - c_3^2c_0 > 0 \tag{10c}$$

Table 1 shows the eigenvalues (roots of the characteristic Eq. 9) obtained by using the Newton-Raphson method for $0.0050 \leq \alpha \leq 0.7000$ with the following sets of system parameters: $\gamma_C = 3.23529$; $\gamma_L = 3.04761$ (equivalently $L_2 = 84\,\text{mH}$, $C_2 = 68\,\text{nF}$ and varying R_N). Since M_J is a real matrix, complex eigenvalues occur in complex conjugate pairs. It can be noted from Table 1 that for the critical value $\alpha = \alpha_c \approx 0.0066$, there are two pairs of complex conjugate eigenvalues, among which a pair with zero real part. This critical value α_c corresponds to the Hopf bifurcation point. Indeed, for values of $\alpha \leq \alpha_c$, P_0 has eigenvalues all with negative real part (i.e. stable spiral point). Eigenvalues with positive real parts are obtained for values of $\alpha \geq \alpha_c$; in this case P_0 is classified as an unstable spiral point. Consequently, (regular or chaotic/hyperchaotic) oscillations generated for

Table 1 Stability of the fixed point P_0 (0, 0, 0, 0)in terms of parameter α The rest of model parameters are defined in the text

Parameter α	Nonlinear resistor $\lvert R_N\rvert = R_1$	Eigenvalues $\lambda_1, \lambda_2, \lambda_3, \lambda_4$	Stability of P_0
0.0050	215740Ω	$-0.0045 \pm 1.0000i$	Stable
		$-0.0026 \pm 3.1400i$	
0.0066	163440Ω	$-0.0037 \pm 1.000i$	Neutral (Hopf bifurcation)
		$\pm 3.1400i$	
0.3000	3595.7Ω	$0.1545 \pm 1.0038i$	Unstable
		$0.4631 \pm 3.0469i$	
0.5400	1997.6Ω	$0.3184 \pm 1.0143i$	Unstable
		$0.8074 \pm 2.8230i$	
0.7000	1541Ω	$0.4709 \pm 1.0266i$	Unstable
		$0.9937 \pm 2.5731i$	

this range of system parameter values are classified as self-excited [21,22].

4 Bifurcation analysis

4.1 Numerical methods

To define different scenarios/routes to chaos in our model, system (4) is solved numerically using the standard fourth-order Runge–Kutta integration algorithm. For each set of parameters used in this paper, the time step is always $\Delta t \leq 0.005$ and the computations are carried out using variables and parameters in extended precision mode. For each parameter setting, the system is integrated for a sufficiently long time and the transient is discarded. Two indicators are exploited to characterize the type of transition leading to chaos. The first indicator is the bifurcation diagram, the second indicator being the graph of three largest Lyapunov exponents' spectra. Concerning the latter case, the dynamics of the system is classified using its Lyapunov exponents which are computed numerically with the help of the reliable algorithm of Wolf et al. [23]. Unlike some other methods, which only compute the largest Lyapunov exponent, the algorithm of Wolf et al. calculates the full spectrum of the Lyapunov exponents and thus allows one to distinguish between chaotic attractors marked by only one positive exponent, and hyperchaotic attractors characterized by more than one positive exponent. Moreover, the Lyapunov dimension of the attractors is obtained according to the definition of Kaplan and Yorke:

$$D_L = k + \frac{1}{|\lambda_{k+1}|}\sum_{i=1}^{k}\lambda_i \tag{10}$$

where k satisfies $\sum_{i=1}^{k}\lambda_i \geq 0$ and $\sum_{i=1}^{k+1}\lambda_i < 0$. Briefly recall that $2 < D_L < 3$ for simple chaos while hyperchaos is characterized with a Lyapunov dimension $D_L > 3.0$.

4.2 Bifurcation with respect to parameter α

In order to investigate the sensitivity of our model with respect to the control parameter α, we fix $\gamma_C = 3.23529$, $\gamma_L = 3.04761$ and α is varied. The structure of the bifurcation diagrams and the corresponding spectrum of three largest Lyapunov exponents are depicted in Fig. 2a–c. Two sets of data are presented. Figure 2a is obtained by plotting the local maxima of the state variable $x_3(t)$ in terms of the control parameter α that is decreased (i.e. R_1 is increased, provided that $\alpha = -\rho/R_N = \rho/R_1$) in tiny steps. The final state at each iteration of the control parameter serves as initial condition for the next iteration. In contrast, Fig. 2b is obtained using the same initial point (0.2, 0.4, −0.2, 0.1) at

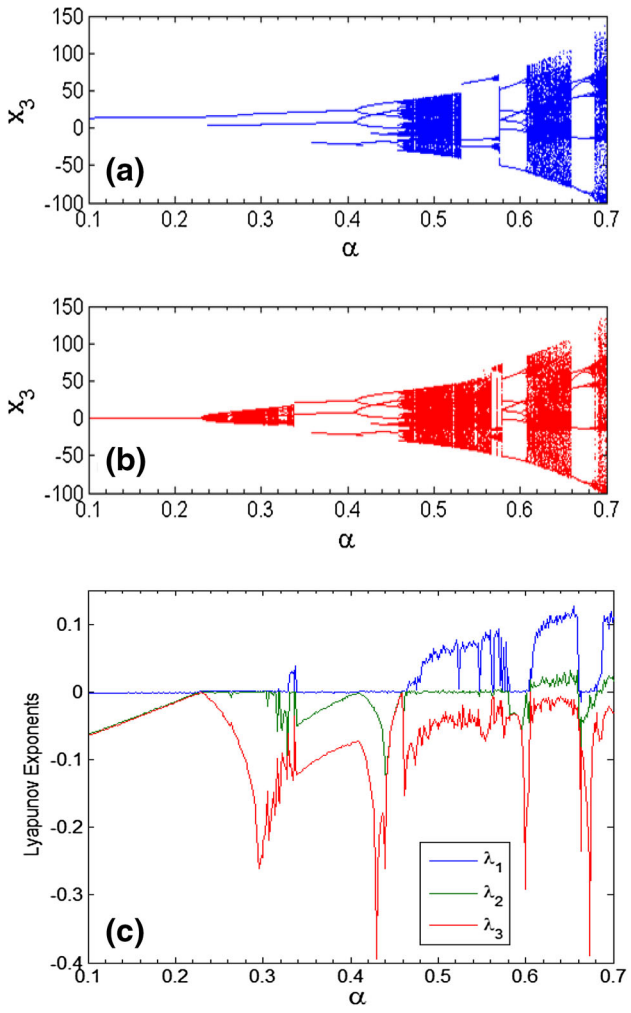

Fig. 2 Bifurcation diagrams (**a**, **b**) showing the coordinates x_3 in terms of the control parameter α and corresponding graphs of three largest Lyapunov exponents (**c**) computed (see text for details of procedure) with : $\gamma_C = 3.23529$; $\gamma_L = 3.04761$

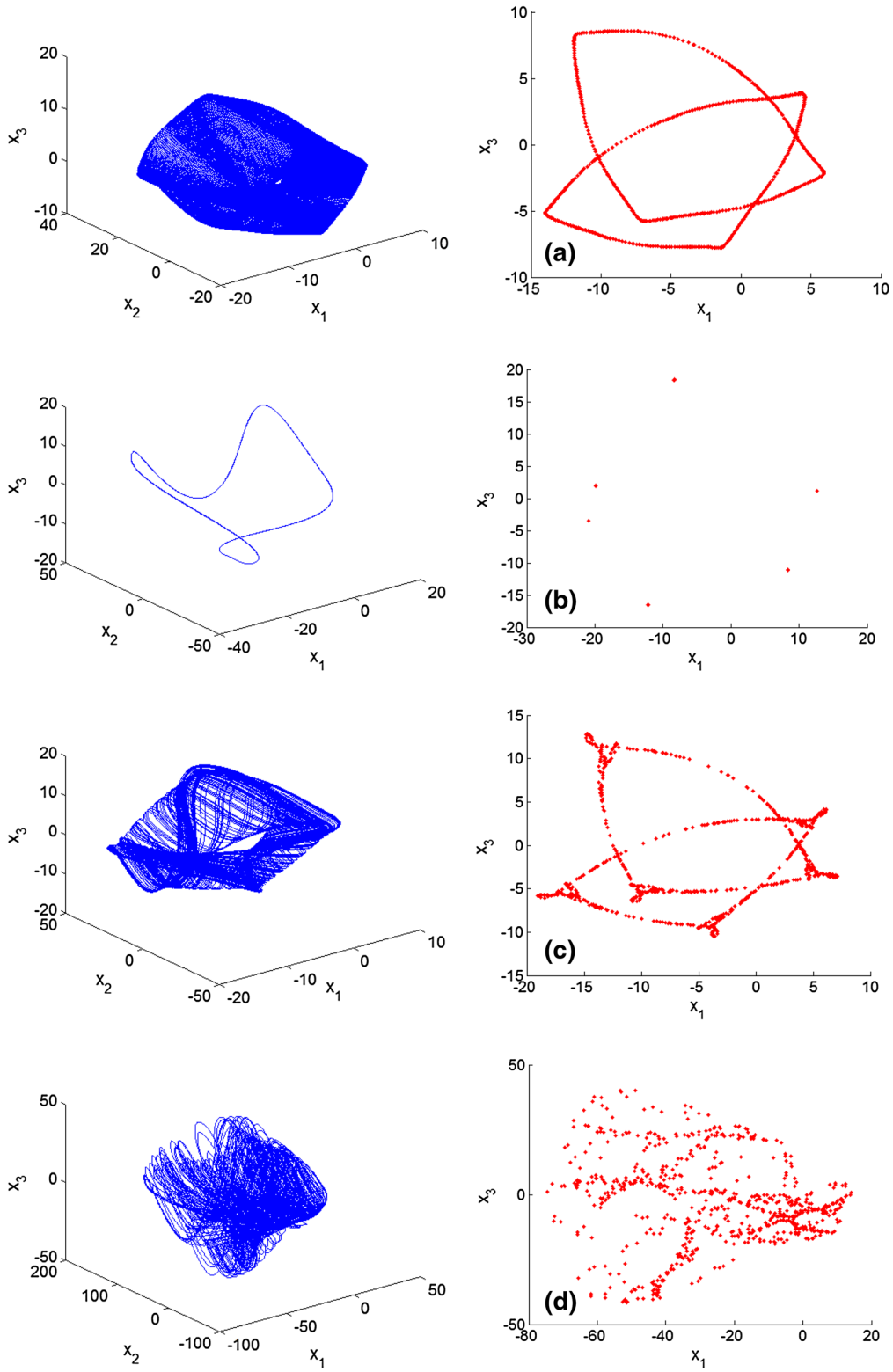

Fig. 3 Typical 3D views of the attractors projected onto the (x_1, x_2, x_3) space and corresponding (*double sided*) Poincaré sections (in the hyperplane $x_2 = 0$) obtained for some specific values of the control parameter α: **a** torus state for $\alpha = 0.30$; **b** periodic attractor for $\alpha = 0.30$; **c** chaos for $\alpha = 0.3375$; **d** chaotic attractor for $\alpha = 0.54$; **e** periodic attractor for $\alpha = 0.54$; **f** hyperchaos for $\alpha = 0.70$. The rest of parameters are those in Fig. 2. Initial conditions $(x_1(0), x_2(0), x_3(0), x_4(0))$ leading to the attractors shown in **a**–**f** are respectively: $(0.20, 0.40, -0.20, 0.10)$, $(20, 40, -20, 10)$, $(20, -40, -20, 10)$, $(20, -40, -20, 10)$, $(20, 40, -20, 10)$ and $(0.20, 0.40, -0.20, 0.10)$

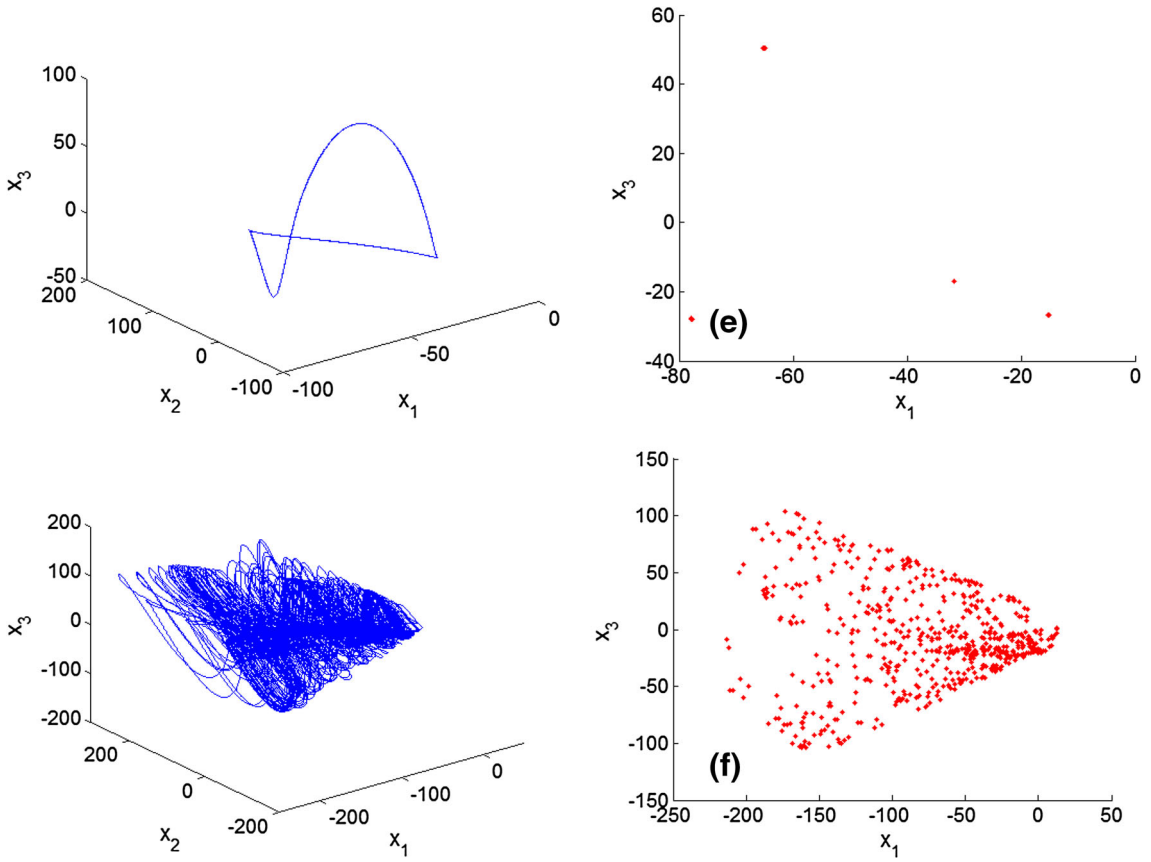

Fig. 3 continued

any iteration of the bifurcation control parameter. From Fig. 2a, the following transitions are observed when the control parameter α is slowly decreased: hyperchaos $\rightarrow$ period-5 $\rightarrow$ hyperchaos $\rightarrow$ period-6 $\rightarrow$ period-3 $\rightarrow$ chaos $\rightarrow$ period-6 $\rightarrow$ periodic-5 $\rightarrow$ periodic-3 $\rightarrow$ period-2 $\rightarrow$ period-1. In other words, the hyperchaos motion is destroyed progressively within the LMT oscillator with respect to the control parameter α. By comparing the diagrams depicted in Fig. 2a, b with Lyapunov exponenents in 2c, intervals of α in which two attractors coexist are clearly identified. Also note the presence of tiny windows of regular/periodic motion in the chaotic and hyperchaotic bands. It can be seen that the bifurcation diagrams well coincide with the spectrum of the Lyapunov exponents. In particular, a good coincidence is observed between band of chaos and windows of regular behavior within those diagrams. Using the same parameter settings in Fig. 2, various numerical computations of phase portraits and corresponding (double sided) Poincaré sections (in the hyperplane $x_2 = 0$) were obtained confirming different transitions depicted previously (see Fig. 3). Typical bi-stable behaviors involving a chaotic attractor and a periodic solution are depicted in Fig. 3c–e. For instance, the phase portrait of Fig. 3d can be obtained under the initial conditions $x_1\,(0) = 20$, $x_2\,(0) = -40$, $x_3\,(0) = -20$ and $x_4\,(0) = 10$; using the initial conditions $x_1\,(0) = 20$, $x_2\,(0) = 40$, $x_3\,(0) = -20$ and $x_4\,(0) = 10$ a completely different solution (i.e. a periodic attractor) is obtained in Fig. 3e. Therefore, considering the set of parameters in Fig. 3c–e and performing a scan of initial conditions [in the (x_2, x_4) plane see Fig. 4], we have defined the domain of initial conditions in which the chaotic solution can be found. In Fig. 4a, b, we present the basin of attraction corresponding to the chaotic solution (blue regions) for two different values of the control parameters (i.e. $\alpha = 0.3375$ and $\alpha = 0.540$). These regions represent initial conditions that lead to chaotic trajectories. The white regions correspond to the regular/periodic orbit.

4.3 Bifurcation with respect to parameters γ_C and γ_L

To evaluate the sensitivity of our model with respect to the control parameter γ_C, we fix $\alpha = 0.55$, $\gamma_L = 3.04761$ and γ_C is varied. Fig. 5a, b show the bifurcation diagrams of the system and corresponding graph of three largest Lyapunov exponents (Fig. 5c) versus the control parameter γ_C obtained using the strategies similar to those described previously. In particular, Fig. 5a is obtained by plotting the local maxima of the state variable $x_3\,(t)$ in terms of the control parameter γ_C that is increased in tiny steps. The final state at each iteration

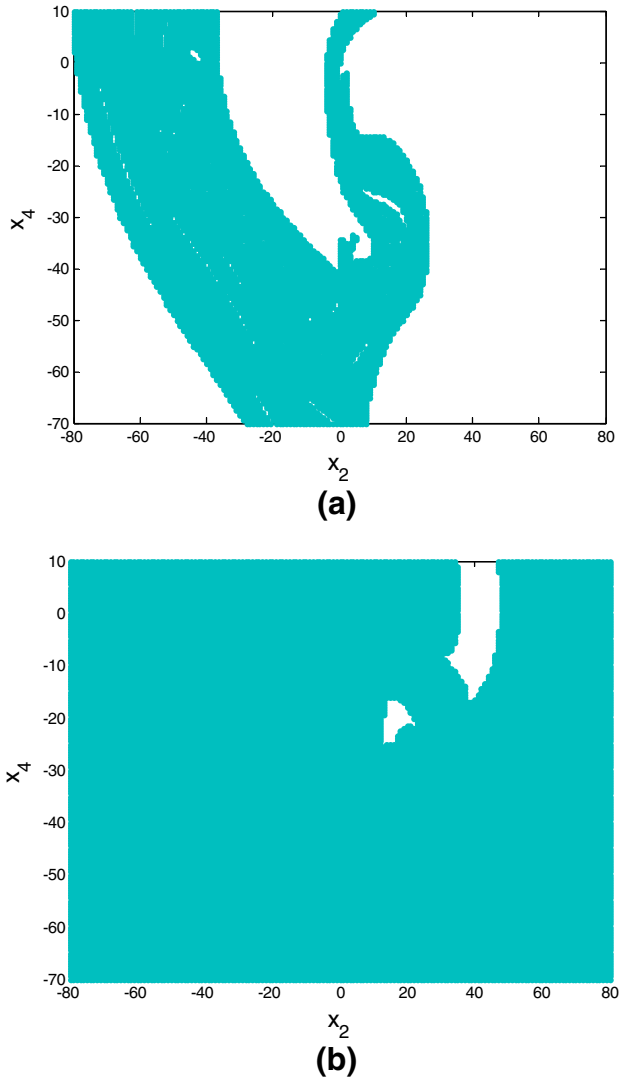

Fig. 4 Structures of the section of the basin of attraction with $(x_1^0, x_3^0) = (20, -20)$, related to the chaotic trajectories depicted in Fig. 3c, d. *White* regions correspond to the periodic solution while blue ones are associated to the chaotic attractor: **a** $\alpha = 0.3375$, **b** $\alpha = 0.54$

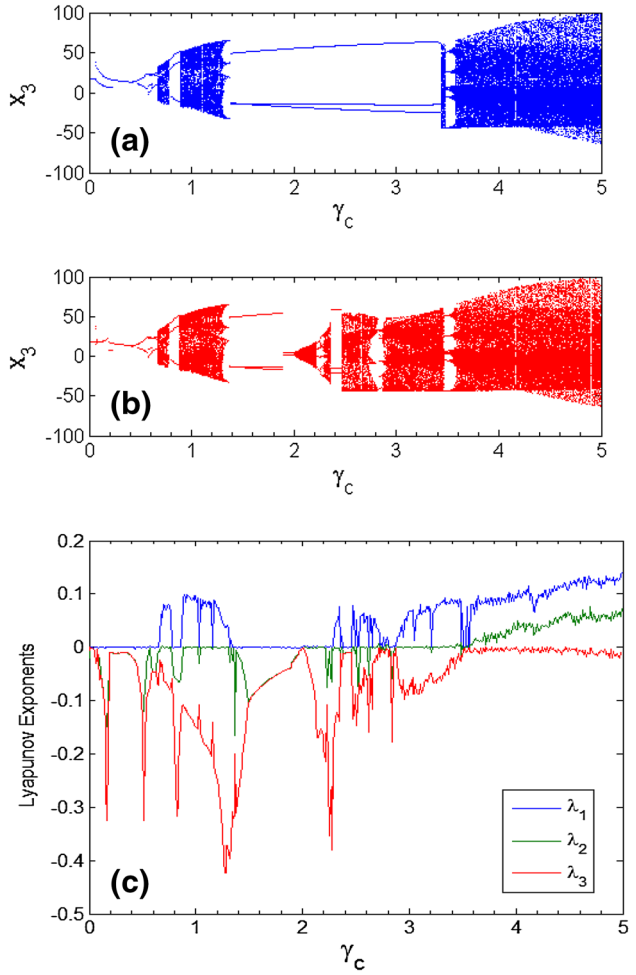

Fig. 5 Bifurcation diagrams (**a**, **b**) showing the coordinates x_3 in terms of the control parameter γ_C and corresponding graphs of three largest Lyapunov exponents (**c**) computed (see text for details of procedure) with: $\alpha = 0.55$; $\gamma_L = 3.04761$

of the control parameter serves as initial condition for the next iteration. In contrast, Fig. 5b is obtained using the same initial point $(0.2, 0.4, -0.2, 0.1)$ at any iteration of the bifurcation control parameter. Once more, the bi-stability property of the system is clearly illustrated by a direct comparison of the diagrams in Fig. 5a and (5b). A stable period-3 orbit coexists with a period-2 orbit, a torus attractor, a period-4 orbit, a chaotic attractor or a period-6 orbit when the control parameter γ_C lies in the window $[1.85,\ 3.40]$. Note the good coincidence between the bifurcation diagrams and the graph of Lyapunov exponents. From Fig. 5c, it can be seen that the system exhibits two positive Lyapunov exponents (i.e. hyperchaos) for values of γ_C approximately greater than the critical value $\gamma_{C\min} = 3.50$. For instance, with $\gamma_C = 4.50$, the spectrum of the Lyapunov exponents is: $\lambda_1 = 0.113$, $\lambda_2 = 0.060$, $\lambda_3 = 0.000$, $\lambda_4 = -19.144$; the corresponding Lyapunov dimension being $D_L = 3.009$.

Figure 6a–c depict the bifurcation diagrams with corresponding graph of three largest Lyapunov exponents plotted against the control parameter γ_L (computed with $\alpha = 0.55$ and $\gamma_C = 3.23529$) with same procedure as in the case of varying γ_C described above. Here the interval of γ_L in which two attractors coexist reduces to a tiny interval located at $\gamma_L \approx 3.0$ while the presence of two positive Lyapunov exponents is observed for values of γ_L satisfying $4.4 \leq \gamma_L \leq 6.0$. As in the previous cases, the bifurcation diagrams are perfectly traced by the graph of three largest Lyapunov exponents. However, it should be stressed that the coexistence of attractors observed in the LMT oscillator has also been observed in various nonlinear systems including laser [24], biological systems [25] and electrical circuits [26], to name a few. This may serve to validate the results obtained in this work. We would like to stress however, that from a practical

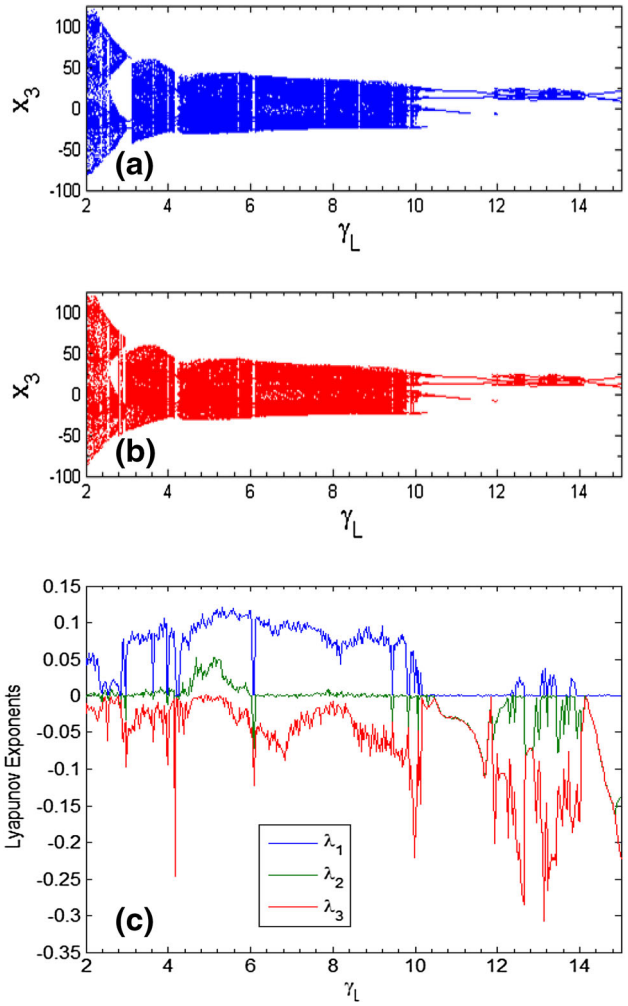

Fig. 6 Bifurcation diagrams (**a**, **b**) showing the coordinates x_3 in terms of the control parameter γ_L and corresponding graphs of three largest Lyapunov exponents (**c**) computed (see text for details of procedure) with: $\gamma_C = 3.23529$; $\alpha = 0.55$

view point; the bi-stability behaviour exhibited by the LMT oscillator for some special sets of its parameters is not desirable and justifies the need for control. A detail study on this direction is beyond the scope of this paper.

5 PSpice simulations

According to the theoretical analysis, the LMT hyperchaotic oscillator can experience very striking and complicated dynamic behaviors. Our aim in this section is to verify the theoretical results obtained previously by performing an experimental study of the LMT hyperchaotic oscillator in Spice [27,28]. Also, it of interest to evaluate the effects of simplifying assumptions adopted during the modeling process on the dynamics of a hardware implementation of the LMT hyperchaotic circuit in PSpice. The main advantage of using PSpice is the possibility of changing initial capacitor voltages as well as initial inductor currents and analyzing the corresponding effect/influence on the dynamics of the complete electronic generator. Thus different coexisting attractors can be tracked/observed in a straightforward way. For this purpose, the schematic diagram of the experimental LMT oscillator (see Fig. 1) is implemented in PSpice. The circuit is built using LM741 op. amplifiers type powered by a symmetric ± 15 V dc voltage source and a general purpose $1N4148$ diode [6]. The rest of circuit components are: $C_1 = 220$ nF, $C_2 = 68$ nF $R_{L1} = 15\Omega$, $R_{L2} = 7.5\Omega$, $R_1 = 10\,\text{k}\Omega$ variable resistor (recall that $R_N = -R_1$), $R_s = 155\Omega$, $R_2 = R_3 = 2\,\text{k}\Omega$, $L_1 = 256$ mH, $L_2 = 84$ mH. The following netlist summarizes the data used in PSpice simulations in case of hyperchaos attractor; the rest of attractors are obtained by simply changing both the values of resistor R_1 and initial conditions as indicated in the caption of Fig. 7:

* Schematics Netlist *	
D_D1	0 $N_0001 D1N4148
R_RS	$N_0001 $N_0002 155
R_RL1	$N_0003 0 15
V_V1	$N_0004 0 15V
V_V2	0 $N_0005 15V
R_RL2	$N_0006 $N_0002 7.5
R_R3	$N_0001 $N_0007 2k
R_R2	$N_0008 $N_0007 2k
X_U1	$N_0001 $N_0008 $N_0004 $N_0005 $N_0007 LM741
R_R1	0 $N_0008 1997.6
L_L2	$N_0011 $N_0006 84mH IC=0.50
C_C1	$N_0011 0 220n IC=-0.998
C_C2	$N_0011 $N_0002 68n IC=0.494
L_L1	$N_0011 $N_0003 256mH IC=-0.252

The bi-stability property of the systems reported during the numerical analysis is confirmed in Spice simulations as well as the scenarios leading to hyperchaos. Sample results are depicted in Fig. 7 where various coexisting states are presented. Figure 7a shows the coexistence of two different attractors (a torus with a periodic orbit) obtained in Spice with different initial points along with their theoretical counterparts. Similarly, a chaotic attractor coexisting with a periodic orbit is depicted in Fig. 7b aside with similar theoretical results. The results in Fig. 7 confirm a good agreement between theoretical and experimental analyses and thereby can be considered to validate the mathematical model proposed in this paper to describe the dynamic behavior of the LMT hyperchaotic oscillator.

6 Concluding remarks

To summarize, this paper has investigated the nonlinear dynamics of a simple 4D hyperchaotic electronic oscilla-

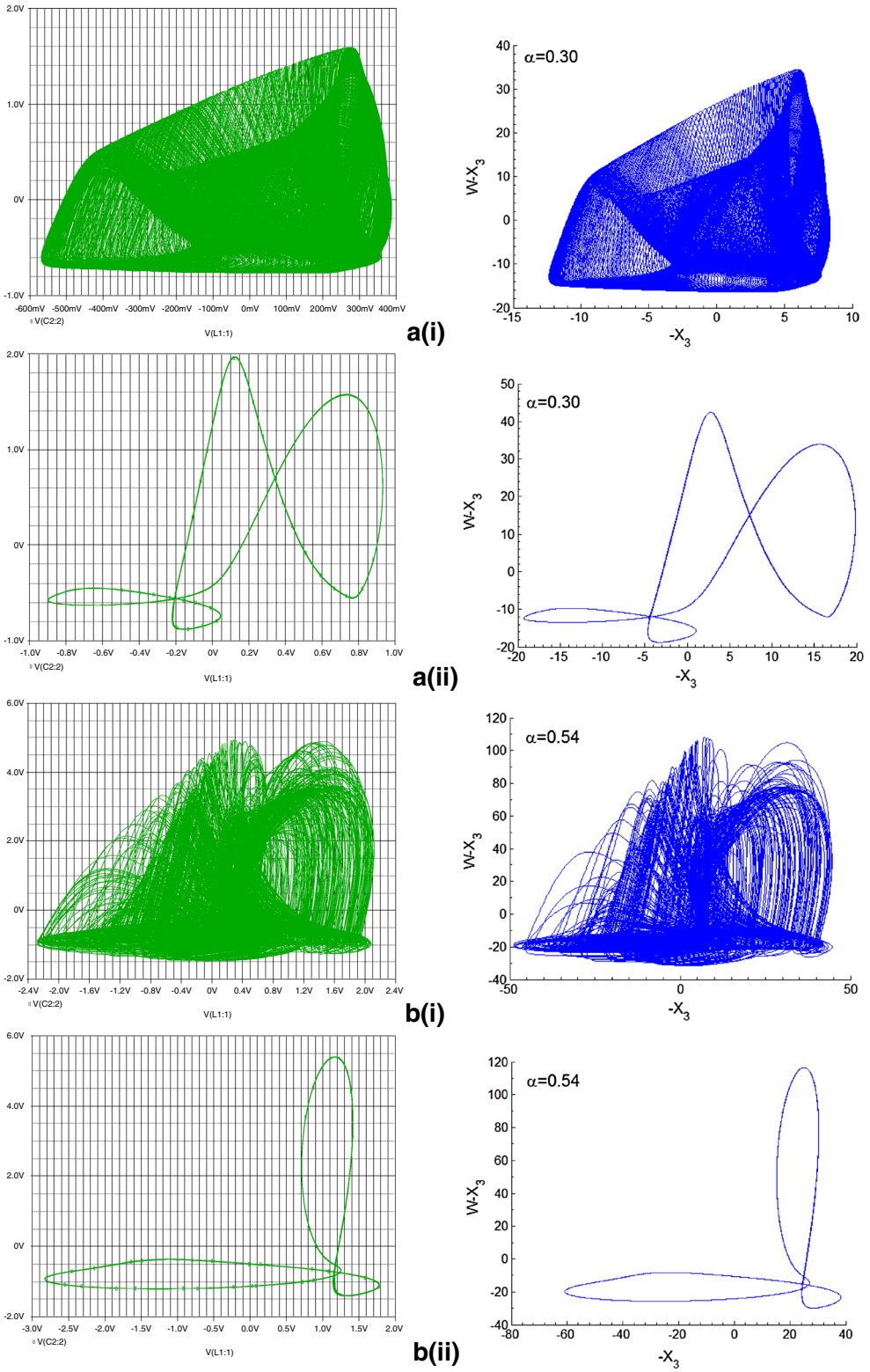

Fig. 7 Comparison between the PSpice simulations results (*left column*) and similar theoretical ones (*right column*) obtained by direct integration of our model in Eq. (4) with the same initial conditions of Fig. 3. The PSpice simulations results ($x = V$ (3) and $y = V$ (2); node 2 and 3 being indicated in Fig. 1 presented in **a(i)**, **a(ii)**, **b(i)** and **b(ii)** are computed using respectively two different values for nonlinear resistor (i.e. $R_1 = -R_N = 3595.7\Omega$ and $R_1 = -R_N = 1997.6\Omega$) and the initial points $\left(I_{L_1}(0), I_{L_2}(0), V_{C_1}(0), V_{C_2}(0)\right)$ as follows: **a(i)** $(0.30A, -0.42A, -0.10V, -0.15V)$, **a(ii)** $(0.30A, -0.42A, 10V, 10V)$, **b(i)** $(0.252A, 0.50A, -0.998V, 0.494V)$ and **b(ii)** $(-0.252A, 0.50A, -0998V, 0494V)$. These two values of the nonlinear resistor R_N correspond to $\alpha = 0.30$ and $\alpha = 0.54$

tor described by a set of coupled four first order differential equations with exponential nonlinearities. The smooth model is advantageous as it provides a close form description of the oscillator's behaviour. The analysis of the bifurcation diagrams and the Lyapunov exponents confirm that the LMT oscillator has extremely complicated dynamics. Some striking scenarios/routes to chaos were depicted including period-adding, period-doubling and torus breakdown route to chaos. The bi-stability property of the system involving the coexistence of different solutions for the same parameters values was also discussed. One of the attractive features of this particular oscillator is the presence of hyperchaotic motion over a broad range of parameter values which might be useful for applications in synchronization and chaos based communication (e.g. Chaotic masking) as well. PSpice based simulations results show a very good agreement with the results obtained by a direct numerical integration of the mathematical model proposed in this paper. This clearly shows that the smooth mathematical model based on the exponential I–V characteristic of the diode is appropriate to capture detailed behaviours of semiconductor diode-based circuits in general [29]. It should be mentioned that the bi-stability property of the LMT oscillator is also found in hardware models of the classic Lorenz oscillator based on AD633 multipliers and op. amplifiers RC integrators [30,31]. We would like to stress that in contrast to the circuit described in [32], the LMT hyperchaos generator includes no hysteresis element. This implies that the presence of such type of element is not necessary for the occurrence of coexisting bifurcations in a nonlinear circuit. A detailed exploration of the parameter space, aimed at establishing all possible parameter ranges over which the chaotic/hyperchaotic region emerges, may be carried out in future work. Also, it should be stressed that the study performed in this work may easily be extended to similar diode-based chaotic and hyperchaotic generators.

References

1. Filali RL, Benrejeb M, Borne P (2004) On observer-based secure communication design using discrete-time hyperchaotic systems. Commun Nonlinear Sci Numer Simul 19:1424–1432
2. Tamasevicius A, Namajunas A, Cenys A (1996) Simple 4D chaotic oscillator. Electron Lett 32(11):957–958
3. Tamasevicius A, Cenys A, Mykolaittis G, Namajunas A, Lindberg E (1997) Hyperchaotic oscillators with gyrators. Electron Lett 33(7):542–544
4. Tamasevicius A, Cenis A (1998) Hyperchaos in dynamical systems with a monoactive degree of freedom. Chaos Solitons Fractals 9(1–2):115–119
5. Murali K, Tamasevicius A, Mykolaitis G, Namajunas A, Lindberg E (2000) Hyperchaos system with unstable oscillators. Nonlinear Phenom Complex Syst 3:7–10
6. Lindberg E, Murali K, Tamasevicius A (2001) Hyperchaotic circuit with damped harmonic oscillators. In: Proceedings on the 2001 IEEE international symposium on circuits and systems, vol 2. pp 759–762
7. Barbara C, Silvano C (2002) Hyperchaotic behaviour of two bi-directionally Chua's circuits. Int J Circuit Theory Appl 30:625–637
8. Cenys A, Tamasevicius A, Baziliauskas A, Krivickas R, Lindberg E (2003) Hyperchaos in coupled Colpitts oscillators. Chaos Solitons Fractals 17:349–353
9. Matsumoto T, Chua LO, Kobayashi K (1996) Hyperchaos: laboratory experiment and numerical confirmation. IEEE Trans Circuits Syst 11:1143–1147
10. Effati S, Saberi Nik H, Jajarmi A (2013) Hyperchaos control of the hyperchaotic chen system by optimal control design. Nonlinear Dyn 73:499–508
11. Rossler OE (1979) An equation for hyperchaos. Phys Lett A 71:155–157
12. Keihui S, Xuan L, Cong Z, Sprott JC (2012) Hyperchaos and hyperchaos control of the sinusoidally forced simplified Lorenz system. Nonlinear Dyn 69:1383–1391
13. Mykolaitis G, Tamasevicius A, Cenis A, Bumeliene S, Anagnostopoulos AN, Kalkan N (2003) Very high and ultrahigh frequency hyperchaotic oscillators with delay line. Chaos Solitons Fractals 17:343–347
14. Hanias MP, Giannaris G, Spyridakis AR (2006) Time series analysis in chaotic diode resonator circuit. Chaos Solitons Fractals 27:569–573
15. Kengne J, Chedjou JC, Kenne G, Kyamakya K (2012) Dynamical properties and chaos synchronization of improved Colpitts oscillators. Commnun Nonlinear Sci Numer Simul 17:2914–2923
16. Kengne J, Chedjou JC, Fono VA, Kyamakya K (2012) On the analysis of bipolar transistor based chaotic circuits: case of a two-stage Colpitts oscillators. Nonlinear Dyn 67:1247–1260
17. Maggio GM, Di Bernardo M, Kennedy MP (2000) Nonsmooth bifurcations in a piecewise-linear model of the Colpitts oscillator. IEEE Trans Circuits Syst I 47:1160–1177
18. Tetsushi U, Akihisa T (2012) Bifurcation analysis of a simple 3D oscillator and chaos synchronization of its coupled systems. Chaos Solitons Fractals 45:1460–1468
19. Maggio GM, De Feo O, Kennedy MP (1999) Nonlinear analysis of the Colpitts oscillator and application to design. IEEE Trans Circuits Syst I Fundam Theory Appl 46:1118–1130
20. Fozin TF, Kengne J, Pelap FB (2014) Theoretical analysis and adaptive synchronization of a 4D hyperchaotic oscillator. J Chaos 429809
21. Leonov GA, Kuznetsov NV (2013) Hidden attractors in dynamical systems. From hidden oscillations in Hilbert–Kolmogorov, Aizerman and Kalman problems to hidden chaotic attractor in Chua circuits. Int J Bifurc Chaos 23(1):1330002
22. Molaie M, Jafari S, Sprott JC, Golpayegani SMRH (2013) Simple chaotic flows with one stable equilibrium. Int J Bifurc Chaos 23(11):1350188
23. Wolf A, Swift JB, Swinney HL, Wastano JA (1985) Determining Lyapunov exponents from time series. Phys D 16:285–317
24. Masoller C (1994) Coexistence of attractors in a laser diode with optical feedback from a large external cavity. Phys Rev A 50:2569–2578
25. Cushing JM, Henson SM, Blackburn CC (2007) Multiple mixed attractors in a competition model. J Biol Dyn 1(4):347–362
26. Vaithianathan V, Veijun J (1999) Coexistence of four different attractors in a fundamental power system model. IEEE Trans Circuits Syst I 46(3):405–409
27. Lindberg E, Murali K, Tamasevicius A (2005) The smallest transistor-based nonautonomous chaotic circuit. IEEE Trans Cicuits Syst 52(10):661–664
28. Hamill DC (1993) Learning about chaotic circuits with SPICE. IEEE Trans Edu 36:28–35

29. Kengne J, Chedjou JC, Fozin TF, Kyamakya K, Kenne G (2014) On the analysis of semiconductor diode based chaotic and hyperchaotic chaotic circuits—a case study. Nonlinear Dyn 77:373–386
30. Cuomo KM, Oppenheim AV (1993) Circuit implementation of synchronized chaos with applications to communications. Phys Rev Lett 71:65
31. Strogatz SH (1994) Nonlinear dynamics and chaos: with applications to physics, biology, chemistry, and engineering. Perseus Books Publishing, New York
32. Suzuki T, Saito T (1994) On fundamental bifurcations from a hysteresis hyperchaos generator. IEEE Trans Circuits Syst I 41:876–884